SCIENCE CHINA
Information Sciences

August 2020, Vol. 63 180302:1–180302:18
https://doi.org/10.1007/s11432-019-2921-x

• RESEARCH PAPER •
Special Focus on mmWave and Terahertz Wireless Communications for B5G/6G

Machine-learning-based high-resolution DOA measurement and robust directional modulation for hybrid analog-digital massive MIMO transceiver

Zhihong ZHUANG[1], Ling XU[1], Jiayu LI[1], Jinsong HU[2], Linlin SUN[1], Feng SHU[1*] & Jiangzhou WANG[3]

[1]*School of Electronic and Optical Engineering, Nanjing University of Science and Technology, Nanjing* 210094*, China;*
[2]*The College of Physics and Information, Fuzhou University, Fuzhou* 350108*, China;*
[3]*School of Engineering and Digital Arts, University of Kent, Canterbury* CT2 7NT*, UK*

Received 29 December 2019/Revised 22 March 2020/Accepted 19 May 2020/Published online 15 July 2020

Abstract At hybrid analog-digital (HAD) transceiver, an improved HAD estimation of signal parameters via rotational invariance techniques (ESPRIT), called I-HAD-ESPRIT, is proposed to measure the direction of arrival (DOA) of a desired user, where the phase ambiguity due to HAD structure is dealt with successfully. Subsequently, a machine-learning (ML) framework is proposed to improve the precision of measuring DOA. Meanwhile, we find that the probability density function (PDF) of DOA measurement error (DOAME) can be approximated as a Gaussian distribution by the histogram method in ML. Then, a slightly large training data set (TDS) and a relatively small real-time set (RTS) of DOA are formed to predict the mean and variance of DOA/DOAME in the training stage and real-time stage, respectively. To improve the precisions of DOA/DOAME, three weight combiners are proposed to combine the-maximum-likelihood-learning outputs of TDS and RTS. Using the mean and variance of DOA/DOAME, their PDFs can be given directly, and we propose a robust beamformer for directional modulation (DM) transmitter with HAD by fully exploiting the PDF of DOA/DOAME, especially a robust analog beamformer on RF chain. Simulation results show that: (1) the proposed I-HAD-ESPRIT can achieve the HAD Cramer-Rao lower bound (CRLB); (2) the proposed ML framework performs much better than the corresponding real-time one without training stage; (3) the proposed robust DM transmitter can perform better than the corresponding non-robust ones in terms of secrecy rate.

Keywords hybrid analog and digital, ESPRIT, statistical learning, DM, robust precoder

Citation Zhuang Z H, Xu L, Li J Y, et al. Machine-learning-based high-resolution DOA measurement and robust directional modulation for hybrid analog-digital massive MIMO transceiver. Sci China Inf Sci, 2020, 63(8): 180302, https://doi.org/10.1007/s11432-019-2921-x

1 Introduction

Direction of arrival (DOA) measurement, also known as direction finding, belongs to one of the most important aspects in array signal processing [1–3]. It is also a classic research field and enjoys a long and successful history [4–6]. Recently, massive multiple input multiple output (MIMO) promises to provide an ultra-high-resolution DOA estimation [7], which makes DOA estimation regain its new life. The need for high resolution DOA estimation always exists because of its wide applications in many practical scenarios such as radar, sonar, seismic exploration, electronic countermeasures, and radio astronomy [8]. More importantly, with the rapid development of some new technologies such as directional modulation

* Corresponding author (email: shufeng0101@163.com)

(DM), device to device (D2D), satellite communications, unmanned aerial vehicle (UAV), fifth generation (5G), and millimeter wave (mmWave) communications, the demand for DOA estimation will emerge as an explosive growth in the near future.

Classic and representative DOA estimation methods are categorized into two main kinds: conventional and subspace methods. Conventional methods first compute a spatial spectrum and then find DOAs by numerical search of local maxima of the spectrum. Typical methods falling in this class are Capon [9] and Bartlett [10] methods. But these methods suffer from angular resolution loss. Alternatively, two classic high-angular-resolution subspace methods such as multiple signal classification (MUSIC) and estimation of signal parameters via rotation invariance techniques (ESPRIT) algorithms are more popular and achieve wide applications [11, 12].

Recently, compressed sensing (CS) was also applied to improve the precision of DOA estimation. In [13], the authors developed an effective sparse representation L1-SVD algorithm, which first used singular value decomposition (SVD) of data matrix to make a reduction of dimensionality and then the problem of DOA estimation was casted a second-order cone (SOC) optimization. In [14], a mixed $l_{2,0}$ approximation DOA algorithm was proposed to solve the joint-sparse recovery problem, which could distinguish closely spaced and highly correlated sources without knowing the number of emitters in advance. The authors in [7] applied deep learning into massive MIMO system to conduct DOA estimation, where real-time value of DOA can be acquired quickly once deep neural network (DNN) is trained well. In [15], an adaptive DOA estimation method, based on convolutional neural network (CNN) with long short term memory, was developed. In [16], the authors extended the CNN-based DOA estimation method for wide-band signal.

However, all these DOA related work considered the fully digital (FD) structure, in which each antenna is equipped with one dedicated RF (radio frequency) chain. If the number of antennas goes to large-scale, it will lead to a significant increase in circuit complexity and energy consumption. Therefore, a hybrid analog-to-digital (HAD) MIMO structure is an good alternative solution to FD due to its low circuit cost and high energy efficiency. The authors in [17] first developed a low-complexity HAD root-MUSIC algorithm in MIMO receive array with phase alignment, which could achieve the Cramer-Rao lower bound (CRLB) of HAD. However, the need for gratuitous subarray calibration information brings more inconvenience for MUSIC-based methods owing to the fact that the phase drifts will reduce the reliability of received data [18]. More importantly, for root-MUSIC-based methods, to resolve multiple RF emitters, the receiver should know the number of incident waves in advance while ESPRIT does not need such a number and is even capable of estimating this number [12].

In this paper, to avoid the disadvantages of MUSIC-based algorithms, an ESPRIT-based DOA estimator is proposed for an HAD receiver. Here, the phase ambiguity is addressed by maximizing the output receive power, which is similar to the root-MUSIC in [17]. However, the kind of methods will face a performance loss. With the help of machine learning framework, we further improve the performance. Subsequently, to obtain more precise variance, we make a further investigation of the statistical feature of DOA measurement errors (DOAMEs) and conduct a weight combination of the DOA means and variances of training date set (TDS) and real-time set (RTS). Since we complete the density estimation of DOA, we then propose a robust beamforming scheme for hybrid DM using the learned values of DOA and the density of DOAME. Before we summarize our main contributions, let us review the literature concerning DM as follows.

As a secure physical-layer transmission technology [19, 20], DM need to know the angle direction information of a desired user in advance, which can be obtained by the preceding methods. And due to its inherent directive property, DM is suitable for line-of-propagation (LoP) channels such as millimeter wave and satellite communications. The existing research work about DM synthesis can be divided into two categories. The first one was based on RF front-end [21–23]. In [21], the authors developed a near-field direct antenna modulation technique using a large amount of reflectors and switches to adjust the amplitude and phase of signal, thus distorting signal constellation severely. In [22], the authors proposed a phased-array-based DM, which produced phase and amplitude of each symbol in desired direction by shifting phase of each array element. Similarly, in [23], an improved enhancing direct antenna modulation was presented by increasing element spacing to improve the direction error rate in desired direction. The

second way of DM synthesis was implemented in baseband with the aid of artificial noise (AN) to disturb the constellation pattern along undesired directions. In [24], the orthogonal vector method with the help of AN was proposed to synthesize the waveform of DM. In [25], a closed-form expression of null-space-projection (NSP) beamformer was derived and a robust DM synthesis was proposed using the rule of conditional minimum mean square error (MMSE) for single-desired-user scenario. Furthermore, in [26, 27], the concept of robust DM was extended to two new scenarios: multi-beaming broadcasting and MU-MIMO, respectively. The authors in [28, 29] utilized relay-aided DM to enhance the physical layer security. In addition, the authors in [28,30,31] extended DM to secure precise wireless transmission (SPWT) scenario. The former achieved the SPWT with the help of multi-relay while the latter adopted a random frequency diverse array plus DM and random subcarrier selection plus DM with the help of AN, respectively. Additionally, DM was utilized to harvest energy by its directional property [29] due to its excellent directive property. In particular, in a massive MIMO scenario, an extremely high energy-efficiency and security for harvesting energy and transmitting confidential messages can be achieved. From this aspect, we will predict the fact that DM will become a dramatically important secure wireless transmission way in the future wireless networks.

However, all the above research works concerning DM focus on fully-digital transmitter, if a massive transmit antenna array is adopted, a hybrid analog and digital DM transmitter is a perfect choice of striking a good balance by taking circuit cost, energy consumption, and computation complexity into account. Traditional research work pertaining to HAD architectures focus on the design of two beamforming matrices including digital precoder and analog precoder at transmitter in [32–38] without considering AN projection. To the best of our knowledge, there is still no scheme of considering HAD and DM to provide a robust secure transmission with low-complexity and low cost in line-of-sight (LoS) channels. Therefore, in this paper, a robust HAD plus DM transmitter is presented with the aid of AN to achieve a robust and secure physical-layer transmission by exploiting the PDF of measured DOA. Our main contributions are summarized as follows:

(1) An ESPRIT-based DOA measurement method for sub-connected HAD receiver is proposed. By utilizing the rotational invariance among each subarray in sub-connected hybrid architecture, the ESPRIT is well applicable to the sub-connected HAD receiver. And the phase ambiguity due to antenna subarray structure is addressed by maximizing the output power over a set of multiple potential solutions induced by periodicity of phase. Meanwhile, we find that the density distribution of DOA or its DOAME can be approximated as a Gaussian distribution via histogram method in machine learning (ML).

(2) To improve the performance of ESPRIT-based DOA measurement method, an ML-based framework is proposed. In this framework, the values of DOA and variances of DOAME can be achieved with maximum likelihood learning from training stage and real-time stage, respectively. And the outcomes from two stages are combined to form new outputs by a weight method, where the weighted factors rely heavily on the receive SNR, and the numbers of TDS, and RTS. In this way, the probability density function (PDF) of DOAME can be directly given. The above process actually is the density estimation, which paves a way to design a robust beamforming method of DM for HAD-MIMO structure.

(3) After learning the mean values of DOAs and PDFs of DOAMEs of desired user, a robust beamformer for DM in HAD MIMO system is designed, which is made up of three beamforming vectors/matrices: digital precoding vector of confidential message in baseband, digital AN projection matrix in baseband, and analog beamforming matrix on RF chain. The first two beamformers are optimized via minimizing the Euclidean distance between the HAD beamforming matrix and corresponding FD precoder, respectively. The robust analog beamforming matrix is designed by making use of conditional expectation. Simulation results reveal that our proposed robust hybrid method performs much better than non-robust beamforming methods in terms of SR (secrecy rate).

The remainder of this paper is organized as follows. Section 2 describes the system models of HAD receiver to learn DOA and HAD DM transmitter to achieve a robust secure transmission. In Section 3, the ESPRIT-based DOA estimator using HAD structure is proposed, the density of DOAMEs is approximately attained by histogram method, and the TDSs of DOA measurements are constructed. Finally, a weight combination between the outputs of TDS and RTS is to yield a more precise mean and variance

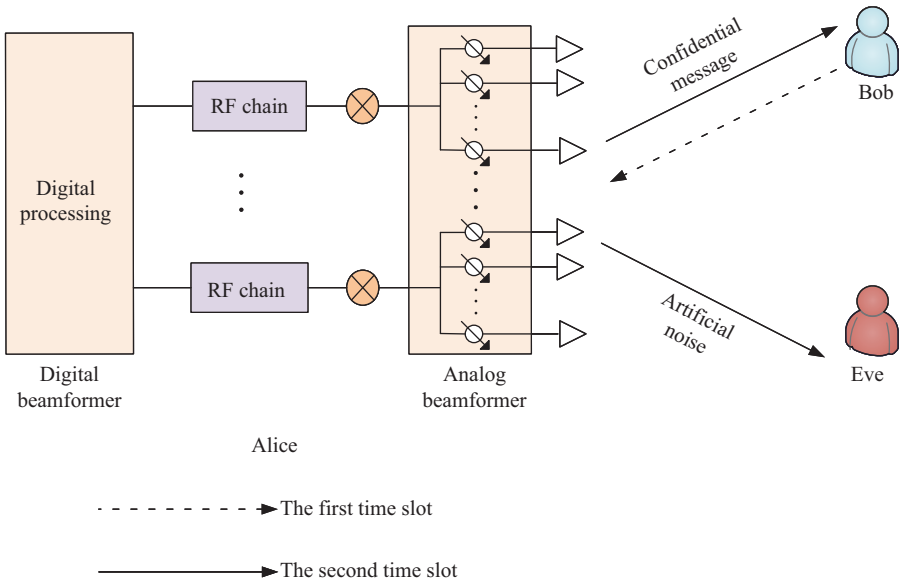

Figure 1 (Color online) Hybrid architecture DOA measurement and DM transceiver.

of DOA. In Section 4, based on conditional expectation, a robust secure beamformer is proposed for DM HAD transmitter with emphasis on analog part. Simulation results will be presented in Section 5. Finally, we draw our conclusion in Section 6.

Notations. throughout the paper, matrices, vectors, and scalars are denoted by letters of bold upper case, bold lower case, and lower case, respectively. $(\cdot)^{\mathrm{T}}$, $(\cdot)^*$, and $(\cdot)^{\mathrm{H}}$ denote transpose, conjugate, and conjugate transpose, respectively. $\|\cdot\|_2$ and $\|\cdot\|_{\mathrm{F}}$ denote the l_2 norm of a vector and Frobenius norm of a matrix, respectively. $\mathrm{tr}(\cdot)$ and $\mathrm{vec}(\cdot)$ are matrix trace and matrix vectorization. $\otimes$ denotes the Kronecker products between two matrices. $\boldsymbol{a}(m1:m2)$ returns a vector consisting of $m1^{\mathrm{th}}$ to $m2^{\mathrm{th}}$ elements in vector $\boldsymbol{a}$.

2 System model

In Figure 1, the schematic diagram of an HAD transceiver is shown. We consider that the practical DM system consists of two steps. Before performing the beamforming operation of DM, the directional angle of desired user or its statistical property is measured in the first time slot. Subsequently, using the measured value of DOA or its statistical property, the beamforming scheme can be well designed in the second time slot. The sub-connected hybrid architecture is adopted here, where the antenna array is made up of K sub-arrays and each sub-array has M antennas. In other words, $N = KM$, where N is the total number of antennas at Alice. Below, we establish the system models of HAD transceiver.

In the first time slot, Alice performs as an HAD receiver, where a narrow-band signal $s(t)\mathrm{e}^{\mathrm{j}w_c t}$ from a far-field emitter Bob impinges on it, while Eve stays silently as a passive eavesdropper. In this case, the received signal is given by

$$\boldsymbol{y}_a(t) = \boldsymbol{F}_{\mathrm{RF}}^{\mathrm{H}}\boldsymbol{a}(\theta)s(t)\mathrm{e}^{\mathrm{j}w_c t} + \boldsymbol{n}(t), \tag{1}$$

where $s(t)$ is the baseband signal, $w_c = 2\pi f_c$ with f_c being carrier frequency, and $\boldsymbol{a}(\theta)$ is the array manifold defined as

$$\boldsymbol{a}(\theta) = \left[1, \mathrm{e}^{\mathrm{j}\frac{2\pi}{\lambda}d\cos\theta}, \ldots, \mathrm{e}^{\mathrm{j}\frac{2\pi}{\lambda}(N-1)d\cos\theta}\right]^{\mathrm{T}}, \tag{2}$$

which is used to estimate the angle range from 0° to 180° and convenient to design beamformer for DM in the following sections. In (1), $\boldsymbol{F}_{\mathrm{RF}}$ is the $N \times K$ analog receive beamforming matrix consisting of

K analog weight vectors $\boldsymbol{f}_k$, with each element having the same amplitude $\frac{1}{\sqrt{M}}$ but different phases, as follows:

$$\boldsymbol{F}_{\mathrm{RF}} = \begin{bmatrix} \boldsymbol{f}_1 & \boldsymbol{0} & \cdots & \boldsymbol{0} \\ \boldsymbol{0} & \boldsymbol{f}_2 & \cdots & \boldsymbol{0} \\ \vdots & \vdots & & \vdots \\ \boldsymbol{0} & \boldsymbol{0} & \cdots & \boldsymbol{f}_K \end{bmatrix}, \tag{3}$$

where $\boldsymbol{f}_k = \frac{1}{\sqrt{M}}[\mathrm{e}^{\mathrm{j}\alpha_{k,1}}, \ldots, \mathrm{e}^{\mathrm{j}\alpha_{k,M}}]^{\mathrm{T}}$. Then, after performing the down-conversion and analog-to-digital conversion (ADC) operations, the receive signal at Alice can be expressed as

$$\boldsymbol{y}_a(n,\theta) = \boldsymbol{F}_{\mathrm{RF}}^{\mathrm{H}}\boldsymbol{a}(\theta)s(n) + \boldsymbol{n}. \tag{4}$$

Finally, after the digital beamforming operation, the received signal can be written as

$$r(n) = \boldsymbol{f}_{\mathrm{BB}}^{\mathrm{H}}\boldsymbol{F}_{\mathrm{RF}}^{\mathrm{H}}\boldsymbol{a}(\theta)s(n) + \boldsymbol{f}_{\mathrm{BB}}^{\mathrm{H}}\boldsymbol{n}. \tag{5}$$

By making use of the above model, we will develop an improved ESPRIT-based DOA estimator for HAD architecture to learn the direction angle of the desired user. The specific DOA estimation process will be presented in Section 3.

After obtaining the value of DOA of Bob, now we show how to implement a DM transmitter using HAD beamforming as indicated in the second time slot. Here, Alice works on transmitter model. The DM transmitter is equipped with N uniformly spaced linear antennas array. The transmitted signal is given by

$$\boldsymbol{s} = \sqrt{\beta P_s}\boldsymbol{V}_{\mathrm{RF}}\boldsymbol{v}_{\mathrm{BB}}x + \sqrt{(1-\beta)P_s}\boldsymbol{V}_{\mathrm{RF}}\boldsymbol{T}_{\mathrm{BB}}\boldsymbol{z}, \tag{6}$$

where P_s is the total transmit power constraint, β denotes the power allocation (PA) factor of confidential messages, and $1-\beta$ stands for the PA factor of AN. Additionally, $\boldsymbol{V}_{\mathrm{RF}} \in \mathbb{C}^{N\times K}$ and $\boldsymbol{v}_{\mathrm{BB}} \in \mathbb{C}^{K\times 1}$ represent the analog and digital beamforming matrices carrying confidential messages to the desired user, respectively. $\boldsymbol{V}_{\mathrm{RF}}$ has the following form

$$\boldsymbol{V}_{\mathrm{RF}} = \begin{bmatrix} \boldsymbol{v}_1 & \boldsymbol{0} & \cdots & \boldsymbol{0} \\ \boldsymbol{0} & \boldsymbol{v}_2 & \cdots & \boldsymbol{0} \\ \vdots & \vdots & & \vdots \\ \boldsymbol{0} & \boldsymbol{0} & \cdots & \boldsymbol{v}_K \end{bmatrix}, \tag{7}$$

where $\boldsymbol{v}_k$ is the analog beamforming vector of subarray k, $\boldsymbol{T}_{\mathrm{BB}} \in \mathbb{C}^{K\times N_s}$ denotes the digital AN projection matrices with constraints $\|\boldsymbol{V}_{\mathrm{RF}}\boldsymbol{T}_{\mathrm{BB}}\|_{\mathrm{F}}^2 = \|\boldsymbol{V}_{\mathrm{RF}}\boldsymbol{v}_{\mathrm{BB}}\|^2 = 1$. $x \sim \mathcal{CN}(0,1)$ and $\boldsymbol{z} \sim \mathcal{CN}(0,\boldsymbol{I})$ are the confidential message and AN interfering the eavesdropper, respectively. Let us define the channel steering vector in free space as

$$\boldsymbol{h}^{\mathrm{H}}(\theta) = \left[\mathrm{e}^{\mathrm{j}(1-\frac{N+1}{2})\frac{2\pi d}{\lambda}\cos(\theta)}, \mathrm{e}^{\mathrm{j}(2-\frac{N+1}{2})\frac{2\pi d}{\lambda}\cos(\theta)}, \ldots, \mathrm{e}^{\mathrm{j}(N-\frac{N+1}{2})\frac{2\pi d}{\lambda}\cos(\theta)}\right]. \tag{8}$$

The received signal at the desired user Bob can be expressed as

$$\begin{aligned} y_b &= \boldsymbol{h}^{\mathrm{H}}(\theta_b)\boldsymbol{s} + n_b \\ &= \sqrt{\beta P_s}\boldsymbol{h}^{\mathrm{H}}(\theta_b)\boldsymbol{V}_{\mathrm{RF}}\boldsymbol{v}_{\mathrm{BB}}x + \sqrt{(1-\beta)P_s}\boldsymbol{h}^{\mathrm{H}}(\theta_b)\boldsymbol{V}_{\mathrm{RF}}\boldsymbol{T}_{\mathrm{BB}}\boldsymbol{z} + n_b, \end{aligned} \tag{9}$$

where n_b is the complex additive white Gaussian noise (AWGN) with $n_b \sim \mathcal{CN}(0,\sigma_d^2)$. Similarly, the received signal at eavesdropper is

$$y_e = \boldsymbol{h}^{\mathrm{H}}(\theta_e)\boldsymbol{s} + n_e$$

$$= \sqrt{\beta P_s}\boldsymbol{h}^{\mathrm{H}}(\theta_e)\boldsymbol{V}_{\mathrm{RF}}\boldsymbol{v}_{\mathrm{BB}}x + \sqrt{(1-\beta)P_s}\boldsymbol{h}^{\mathrm{H}}(\theta_e)\boldsymbol{V}_{\mathrm{RF}}\boldsymbol{T}_{\mathrm{BB}}\boldsymbol{z} + n_e, \tag{10}$$

where n_e is the complex AWGN following $n_e \sim \mathcal{CN}(0, \sigma_{\mathrm{e}}^2)$. In particular, it is noted that Eve is assumed to be a passive eavesdropper in our paper. According to (7), the achievable rate of the desired user Bob is

$$R_b = \log_2\left(1 + \frac{\beta P_s \|\boldsymbol{h}^{\mathrm{H}}(\theta_b)\boldsymbol{V}_{\mathrm{RF}}\boldsymbol{v}_{\mathrm{BB}}\|^2}{(1-\beta)P_s\|\boldsymbol{h}^{\mathrm{H}}(\theta_b)\boldsymbol{V}_{\mathrm{RF}}\boldsymbol{T}_{\mathrm{BB}}\|^2 + \sigma_b^2}\right). \tag{11}$$

Similarly, the achievable rate of eavesdropper is

$$R_e = \log_2\left(1 + \frac{\beta P_s \|\boldsymbol{h}^{\mathrm{H}}(\theta_e)\boldsymbol{V}_{\mathrm{RF}}\boldsymbol{v}_{\mathrm{BB}}\|^2}{(1-\beta)P_s\|\boldsymbol{h}^{\mathrm{H}}(\theta_e)\boldsymbol{V}_{\mathrm{RF}}\boldsymbol{T}_{\mathrm{BB}}\|^2 + \sigma_{\mathrm{e}}^2}\right). \tag{12}$$

Then the R_S can be defined as the rate difference between R_b and R_e:

$$R_S = \max\{0, R_b - R_e\}. \tag{13}$$

3 Proposed ML-based framework for DOA estimation using HAD structure

In this section, we improved the ESPRIT-based DOA estimator in HAD structure. By maximizing the receive power over a set of potential angles, the problem of phase ambiguity triggered by HAD structure is addressed well. Using this improved ESPRIT-based DOA estimator and histogram method in ML, we find an important fact: the DOAME obeys a Gaussian distribution. Then, TDS is constructed. Via ML framework, the value of DOA and its density is inferred from this TDS and the following RTS.

3.1 Improved ESPRIT-based HAD DOA estimator

First, let us assume the phases of all elements of analog beamforming matrix are equal to zeros, that is, each analog subarray satisfies

$$\boldsymbol{f}_k = \frac{1}{\sqrt{M}}[1, \ldots, 1]^{\mathrm{T}}. \tag{14}$$

Then, in accordance with Eq. (4), we can directly obtain the output vector after analog beamforming as follows:

$$\begin{aligned}\boldsymbol{y}_a(n) &= \boldsymbol{F}_{\mathrm{RF}}^{\mathrm{H}}\boldsymbol{a}(\theta)s(n) + \boldsymbol{n}\\ &= \frac{1}{\sqrt{M}}\begin{bmatrix} 1\cdots 1 & \mathbf{0} & \cdots & \mathbf{0} \\ \mathbf{0} & 1\cdots 1 & \cdots & \mathbf{0} \\ \vdots & \vdots & & \vdots \\ \mathbf{0} & \mathbf{0} & \cdots & 1\cdots 1 \end{bmatrix}\boldsymbol{a}(\theta)s(n) + \boldsymbol{n}\\ &= \frac{1}{\sqrt{M}}f(\theta)\boldsymbol{a}_K(\theta)s(n) + \boldsymbol{n},\end{aligned} \tag{15}$$

where

$$f(\theta) = \sum_{m=0}^{M-1} \mathrm{e}^{\mathrm{j}\frac{2\pi}{\lambda}Md\cos\theta} = \frac{1 - \mathrm{e}^{\mathrm{j}2\pi/\lambda Md\cos\theta}}{1 - \mathrm{e}^{\mathrm{j}2\pi/\lambda d\cos\theta}}, \tag{16}$$

and

$$\boldsymbol{a}_K(\theta) = \left[1, \mathrm{e}^{\mathrm{j}\frac{2\pi}{\lambda}Md\cos\theta}, \ldots, \mathrm{e}^{\mathrm{j}\frac{2\pi}{\lambda}(K-1)Md\cos\theta}\right]^{\mathrm{T}}. \tag{17}$$

Let $\boldsymbol{a}_D(\theta) = \frac{1}{\sqrt{M}}f(\theta)\boldsymbol{a}_K(\theta)$, then $\boldsymbol{y}_a(n)$ can be recasted as

$$\boldsymbol{y}_a(n) = \boldsymbol{a}_D(\theta)s(n) + \boldsymbol{n}. \tag{18}$$

Next, we adopt ESPRIT to estimate the directional angle of emitter. We choose the first $K-1$ sub-array of antennas to be Array 1, and choose the last $K-1$ sub-array of antennas to be Array 2, then the output can be expressed as

$$\boldsymbol{y}_{a1}(n) = \boldsymbol{a}_{D1}(\theta)s(n) + \boldsymbol{n}_1, \tag{19}$$

and

$$\boldsymbol{y}_{a2}(n) = \boldsymbol{a}_{D2}(\theta)s(n) + \boldsymbol{n}_2 = \boldsymbol{a}_{D1}(\theta)\boldsymbol{\Phi}s(n) + \boldsymbol{n}_2, \tag{20}$$

respectively, where

$$\boldsymbol{a}_{D1}(\theta) = \frac{f(\theta)}{\sqrt{M}}\left[1, \mathrm{e}^{\mathrm{j}\frac{2\pi}{\lambda}Md\cos\theta}, \ldots, \mathrm{e}^{\mathrm{j}\frac{2\pi}{\lambda}(K-2)Md\cos\theta}\right]^{\mathrm{T}}, \tag{21}$$

and $\boldsymbol{\Phi} = \mathrm{diag}\{\mathrm{e}^{\mathrm{j}\frac{2\pi}{\lambda}Md\cos\theta}\}$. By computing the covariance matrix of $\boldsymbol{y}_{a1}(n)$ and $\boldsymbol{y}_{a2}(n)$, we can obtain the signal spaces $\boldsymbol{E}_1$ and $\boldsymbol{E}_2$. Because of the translational displacement, there must exit a non-singular transformation matrix $\boldsymbol{\Psi}$ such that

$$\boldsymbol{E}_1\boldsymbol{\Psi} = \boldsymbol{E}_2, \tag{22}$$

and there must exit a non-singular transformation matrix $\boldsymbol{T}$ such that

$$\boldsymbol{E}_1 = \boldsymbol{a}_{D1}\boldsymbol{T}, \quad \boldsymbol{E}_2 = \boldsymbol{a}_{D1}\boldsymbol{\Phi}\boldsymbol{T}. \tag{23}$$

According to Eqs. (22) and (23), There exists a crucial relationship

$$\boldsymbol{T}\boldsymbol{\Psi}\boldsymbol{T}^{-1} = \boldsymbol{\Phi}. \tag{24}$$

Therefore, it is evident that the eigenvalues of $\boldsymbol{\Psi}$ are equal to the diagonal elements of $\boldsymbol{\Phi}$, i.e.,

$$\lambda_\Psi = \exp\left\{\mathrm{j}\frac{2\pi}{\lambda}Md\cos\theta\right\}. \tag{25}$$

Now the problem is how to calculate the rotation operator $\boldsymbol{\Psi}$. Next, we use the total least-squares method in [12] to estimate $\boldsymbol{\Psi}$. The correlation matrix of the entire antenna array is

$$\boldsymbol{R}_{yy} = E[\boldsymbol{y}_a(n)\boldsymbol{y}_a^{\mathrm{H}}(n)] \approx \frac{1}{L}\{\boldsymbol{Y}_a\boldsymbol{Y}_a^{\mathrm{H}}\} \approx \boldsymbol{a}_D\sigma_s^2P_b^2\boldsymbol{a}_D^{\mathrm{H}} + \sigma_n^2\boldsymbol{I}_K, \tag{26}$$

where $\boldsymbol{Y}_a = [\boldsymbol{y}_a(1), \boldsymbol{y}_a(2), \ldots, \boldsymbol{y}_a(L)]$ is the matrix of spatial-time sampling points. The correlation matrix of the entire antenna array has K eigenvalues, and the associated K eigenvectors $\boldsymbol{E} = [\boldsymbol{e}_1, \boldsymbol{e}_2, \ldots, \boldsymbol{e}_K]$. Signal subspace $\boldsymbol{E}_s$ consists of the eigenvectors corresponding to the largest eigenvalues of the matrix $\boldsymbol{R}_{yy}$. Since signal spaces $\boldsymbol{E}_1$ and $\boldsymbol{E}_2$ can be constructed from the entire antennas array signal space $\boldsymbol{E}_s$, we choose the first $K-1$ rows of $\boldsymbol{E}_s$ to construct $\boldsymbol{E}_1$, and similarly, the last $K-1$ rows to compose $\boldsymbol{E}_2$. Next, we utilize signal subspaces to construct a 2×2 matrix.

$$\boldsymbol{C} = \begin{bmatrix}\boldsymbol{E}_1^{\mathrm{H}}\\ \boldsymbol{E}_2^{\mathrm{H}}\end{bmatrix}[\boldsymbol{E}_1\boldsymbol{E}_2] = \boldsymbol{E}_c\Lambda\boldsymbol{E}_c^{\mathrm{H}}, \tag{27}$$

where $\boldsymbol{E}_c$ can be derived from the EVD (eigen value decomposition) of matrix $\boldsymbol{C}$ and $\Lambda = \mathrm{diag}\{\lambda_1, \lambda_2\}$. Furthermore, $\boldsymbol{E}_c$ can be decomposed into four subarrays as follows:

$$\boldsymbol{E}_c = \begin{bmatrix}\boldsymbol{E}_{11} & \boldsymbol{E}_{12}\\ \boldsymbol{E}_{21} & \boldsymbol{E}_{22}\end{bmatrix}. \tag{28}$$

Then, we can obtain the rotation operator $\boldsymbol{\Psi}$,

$$\boldsymbol{\Psi} = -\boldsymbol{E}_{12}\boldsymbol{E}_{22}^{-1}. \tag{29}$$

By calculating the eigenvalue λ_Ψ of $\boldsymbol{\Psi}$, the angle of emitter estimated by traditional ESPRIT method is

$$\hat{\theta} = \arccos\left(\frac{\lambda \arg(\lambda_\Psi)}{2\pi M d}\right). \tag{30}$$

However, the periodicity in Eq. (25) generates an effect of phase blurring, which makes estimated angle no longer the expression in Eq. (30), thus, we need to extend the estimated angle to a set of potential solutions:

$$\hat{\Theta} = \{\hat{\theta}_i, i \in 0, 1, \ldots, M-1\}, \tag{31}$$

where

$$\hat{\theta}_i = \arccos\left(\frac{\lambda(\arg(\lambda_\Psi) + 2\pi i)}{2\pi M d}\right). \tag{32}$$

According to the criterion of phase alignment, we set the phase of the m phase shifter of each analog subarray as $\alpha_m = \frac{2\pi}{\lambda}(m-1)Md\sin\theta$, and the phase of k element in digital beamforming vector which connects to the k RF chain as $\alpha_k = \frac{2\pi}{\lambda}(k-1)Md\sin\theta$. Then, computing the receive signals power corresponding to the M angles individually, we choose the angle which yields the maximum value of P_r as the optimal one.

$$\hat{\theta} = \arg\min_{\hat{\theta}_i \in \hat{\Theta}} P_r(\hat{\theta}_i) = \frac{1}{LN^2}\sum_{n=1}^{L}(r(n)r(n)^{\mathrm{H}}), \tag{33}$$

where

$$\begin{aligned} r(n) &= \boldsymbol{f}_{\mathrm{BB}}^{\mathrm{H}} y_a(n) = \sum_{k=1}^{K} \mathrm{e}^{-\mathrm{j}\alpha_k} y_a(n) \\ &= \frac{1}{\sqrt{M}} s(n) \sum_{k=1}^{K} \mathrm{e}^{\mathrm{j}\frac{2\pi}{\lambda}(k-1)Md(\cos\theta - \cos\hat{\theta}_i)} \times \sum_{m=1}^{M} \mathrm{e}^{\mathrm{j}\frac{2\pi}{\lambda}(m-1)d(\cos\theta - \cos\hat{\theta}_i)} + \sum_{k=1}^{K} \mathrm{e}^{-\mathrm{j}\frac{2\pi}{\lambda}(k-1)Md\cos\hat{\theta}_i} n. \end{aligned} \tag{34}$$

Since we have obtained the value of DOA of incoming signal, we can further estimate the SNR of incoming signal. Given the estimated angle $\hat{\theta}$, the analog beamforming vector of each subarray can be designed as

$$\hat{\boldsymbol{f}}_k = \frac{1}{\sqrt{M}}\left[\mathrm{e}^{\mathrm{j}\frac{2\pi}{\lambda}((k-1)M+1)d\cos\hat{\theta}}, \ldots, \mathrm{e}^{\mathrm{j}\frac{2\pi}{\lambda}((k-1)M+M)d\cos\hat{\theta}}\right]^{\mathrm{T}}. \tag{35}$$

Then, after the analog beamforming vector $\hat{\boldsymbol{f}}_k$ is performed in RF chain, the output signal of subarray k can be given by

$$\hat{y}_{a,k}(n) = \hat{\boldsymbol{f}}_k^{\mathrm{H}} \boldsymbol{a}_k(\theta) s(n) + n. \tag{36}$$

If the estimated angle $\hat{\theta}$ is equal to the exact angle θ, then $\hat{\boldsymbol{f}}_k^{\mathrm{H}} \boldsymbol{a}_k(\theta) = 1$, and Eq. (36) can be recasted as

$$\hat{y}_{a,k}(n) = s(n) + n, \tag{37}$$

which yields the output vector of all subarrays:

$$\hat{\boldsymbol{y}}_a(n) = [\hat{y}_{a,1}(n), \hat{y}_{a,2}(n), \ldots, \hat{y}_{a,K}(n)]^{\mathrm{T}}. \tag{38}$$

Then we have the overall estimated SNR $\hat{\rho}$ in HAD architecture as follows:

$$\hat{\rho} = \frac{\hat{\boldsymbol{y}}_a(n)^{\mathrm{T}} \hat{\boldsymbol{y}}_a(n)^* - K\sigma_n^2}{K\sigma_n^2}, \tag{39}$$

where σ_n^2 is taken to be the least eigen-value of matrix (26). Until now, we complete the DOA and SNR estimate by the improved ESPRIT, called improved HAD-ESPRIT (I-HAD-ESPRIT) in what follows.

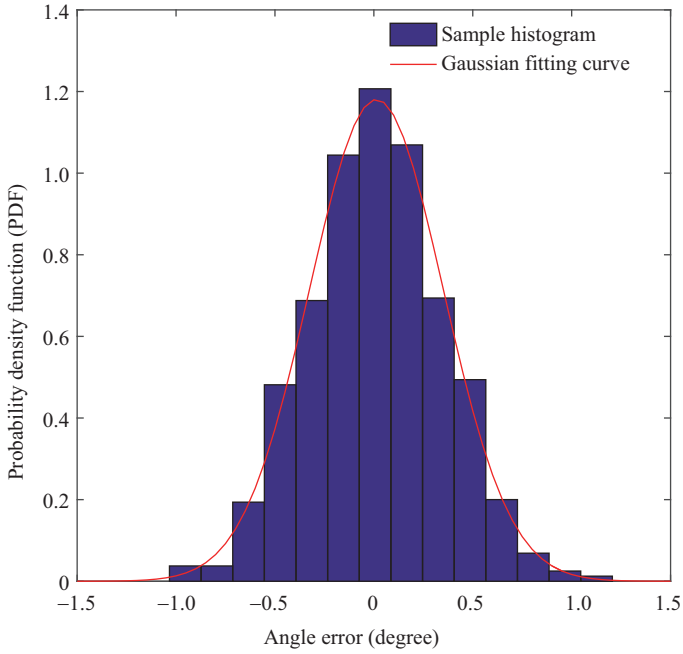

Figure 2 (Color online) DOA measurement error.

3.2 Proposed ML-based DOA and its density estimation

Owing to the effect of channel noise or co-channel signals, there exists DOAME in the estimated DOA in the preceding subsection. Considering DOAME, the estimated angle can be modeled as

$$\hat{\theta}(n) = \theta + \Delta\theta(n), \quad n = 1, \ldots, N_{\mathrm{DOA}}, \tag{40}$$

where $\hat{\theta}(n)$ represents the practical observation angle, θ is the ideal angle we want to obtain, and $\Delta\theta(n)$ is the measurement error between the ideal angle and measured one, $n = 1, 2, \ldots,$ N_{DOA} denotes the number of DOA measurements.

Using the proposed I-HAD-ESPRIT in the preceding subsection repeatedly for several hundreds or thousands, Figure 2 depicts the histogram of DOAME $\Delta\theta(n)$ provided that $N = 32$, $M = 4$, and SNR $=$ 0 dB. From this figure, we can find the important fact that the measured value of DOAME approximately obeys a Gaussian distribution with zero mean.

$$f(\Delta\theta(n)) = \frac{1}{\sqrt{2\pi\sigma^2}} \exp\left\{-\frac{1}{2\sigma^2}(\Delta\theta(n))^2\right\}. \tag{41}$$

If we can learn its variance, then we can give its density function. This is just the density estimation in ML field. Below, we will show how to infer the density of DOAME and improve the accuracy of DOA measurement by making use of ML-based framework.

In practice, a rapid real-time or on-line DOA measurement is required in order to quickly locate the position of emitter, especially in military field. Thus, it is not allowable to take too many time slots. This means that the offline training is very important to infer the density of DOAME and improve the accuracy of DOA measurement. First, the TDS of DOA measurements is offline constructed by using the proposed I-HAD-ESPRIT in the previous subsection. Let us define the TDS as $S_{\mathrm{TDS}} = \{\tilde{\theta}_1, \tilde{\theta}_2, \ldots, \tilde{\theta}_{N_{\mathrm{TDS}}}\}$, where N_{TDS} stands for the number of elements in TDS.

Considering that the DOA measurement is approximated as a Gaussian distribution and in terms of the learning rule of maximum likelihood in [39], we have its mean

$$\hat{\theta}_{\mathrm{TDS}} = \frac{1}{N_{\mathrm{TDS}}} \sum_{\tilde{\theta}_i \in S_{\mathrm{TDS}}} \tilde{\theta}_i, \tag{42}$$

and sampling variance

$$\hat{\sigma}^2_{\rm TDS} = \frac{1}{N_{\rm TDS}-1}\sum_{i=1}^{N_{\rm TDS}}(\tilde{\theta}_i - \hat{\theta}_{\rm TDS})^2 \tag{43}$$

in the training stage. Similarly, in the real-time measuring stage, we have

$$\hat{\theta}_{\rm RTS} = \frac{1}{N_{\rm RTS}}\sum_{\tilde{\theta}_i \in S_{\rm RTS}}\tilde{\theta}_i, \tag{44}$$

and real-time variance

$$\hat{\sigma}^2_{\rm RTS} = \frac{1}{N_{\rm RTS}-1}\sum_{i=1}^{N_{\rm RTS}}(\tilde{\theta}_i - \hat{\theta}_{\rm RTS})^2. \tag{45}$$

If Bob keeps fixed or moves away from Alice along the fixed desired direction during both offline and online periods, then we call this scenario a stable state. Clearly, the above two estimated values of mean and variance can be exploited to improve the accuracy of DOA measurement mean and variance. Conversely, if Bob moves fast away from the desired direction, we call this situation as a moving state. In such a situation, at least the estimated variance during the training stage can be used to improve the accuracy of DOA measurement variance by predicting the variance of real-time measuring stage. In what follows, we discuss the two situations. In the stable state, Alice does not need to adjust its beamforming direction. However, in the moving state, Alice is required to adjust its beam direction to follow the real-time varying angle of the desired user.

Owing to the two important facts: the SNR of training stage may be different from the SNR of real-time measuring stage, and the number $N_{\rm TDS}$ of elements in TDS is also possibly different from that $N_{\rm RTS}$ in RTS, we should take the two factors into account when we combine the learning output of the two sets. In general, $N_{\rm TDS} \gg N_{\rm RTS}$. In the stable state, the weight output of means and variances due to TDS and RTS are given by

$$\hat{\theta}_{\rm ML} = \alpha_1\hat{\theta}_{\rm TDS} + \alpha_2\hat{\theta}_{\rm RTS} = \theta + \delta\theta_{\rm ML} \tag{46}$$

with the constraint $\alpha_1 + \alpha_2 = 1$ with $\alpha_1 \geqslant 0$ and $\alpha_2 \geqslant 0$. In the above equation, α_1 and α_2 depends mainly on the following factors: $\hat{\rho}_{\rm TDS}$, $\hat{\rho}_{\rm RTS}$, $N_{\rm TDS}$, and $N_{\rm RTS}$, where $\hat{\rho}_{\rm TDS}$, and $\hat{\rho}_{\rm RTS}$ are the receive SNRs at Alice in the training and real-time measuring stages, respectively. Based on this, we propose three convex weight combinators with weight factors as follows:

$$\alpha_1 = \frac{\hat{\rho}_{\rm TDS}}{\hat{\rho}_{\rm TDS}+\hat{\rho}_{\rm RTS}}, \quad \alpha_2 = \frac{\hat{\rho}_{\rm RTS}}{\hat{\rho}_{\rm TDS}+\hat{\rho}_{\rm RTS}}, \tag{47}$$

$$\alpha_1 = \frac{N_{\rm TDS}}{N_{\rm TDS}+N_{\rm RTS}}, \quad \alpha_2 = \frac{N_{\rm RTS}}{N_{\rm TDS}+N_{\rm RTS}}, \tag{48}$$

and

$$\alpha_1 = \frac{\hat{\rho}_{\rm TDS}\cdot N_{\rm TDS}}{\hat{\rho}_{\rm TDS}\cdot N_{\rm TDS}+\hat{\rho}_{\rm RTS}\cdot N_{\rm RTS}}, \quad \alpha_2 = \frac{\hat{\rho}_{\rm RTS}\cdot N_{\rm RTS}}{\hat{\rho}_{\rm TDS}\cdot N_{\rm TDS}+\hat{\rho}_{\rm RTS}\cdot N_{\rm RTS}}, \tag{49}$$

respectively. Here, for the sake of convenience, in what follows, Eqs. (47)–(49) are called the proposed weight methods, respectively. Similarly, we have the corresponding weight combiners for DOA variance estimation:

$$\hat{\sigma}^2_{\rm ML} = \alpha_1\tilde{\sigma}^2_{\rm TDS} + \alpha_2\hat{\sigma}^2_{\rm NDS}, \tag{50}$$

where the weight parameters α_1 and α_2 are given by (47)–(49), respectively. And

$$\tilde{\sigma}^2_{\rm TDS} = \frac{\hat{\rho}_{\rm TDS}}{\hat{\rho}_{\rm RTS}}\hat{\sigma}^2_{\rm TDS}. \tag{51}$$

In the moving scenario, it is particularly noted that the learned variance in training stage has an intimately direct relationship with real-time measuring one. At least it is used to predict the variance of the real-time measuring case in terms of their SNRs, and numbers of RTS and TDS. However, due to moving, the direction angles of Bob and Eve will change with time, the learned DOA mean in RTS will be independent of the learned DOA mean from TDS. In other words, the learned DOA mean from RTS will be used as the final learned DOA. In such a situation, the weight factors α_1 and α_2 in (46) are set to 1 and 0, respectively.

4 Proposed robust HAD beamformer for DM

In the above section, we have attained the measured value $\hat{\theta}_{\mathrm{ML}}$ and variance $\hat{\sigma}^2_{\mathrm{ML}}$ of DOA, then we have the ML-based DOA output modeled as

$$\theta = \hat{\theta}_{\mathrm{ML}} - \Delta\hat{\theta} \tag{52}$$

with its PDF as follows:

$$f(\theta; \hat{\theta}_{\mathrm{ML}}, \hat{\sigma}^2_{\mathrm{ML}}) = \frac{1}{\sqrt{2\pi\hat{\sigma}^2_{\mathrm{ML}}}} \exp\left\{-\frac{1}{2\hat{\sigma}^2_{\mathrm{ML}}}(\theta - \hat{\theta}_{\mathrm{ML}})^2\right\}, \tag{53}$$

which yields the PDF of DOAME:

$$f(\Delta\hat{\theta}; \hat{\sigma}^2_{\mathrm{ML}}) = \frac{1}{\sqrt{2\pi\hat{\sigma}^2_{\mathrm{ML}}}} \exp\left\{-\frac{1}{2\hat{\sigma}^2_{\mathrm{ML}}}(\Delta\hat{\theta})^2\right\}. \tag{54}$$

Considering that the DOAME falls into the interval $[\pi, \pi]$, similar to [26, 29], the PDF of DOAME can be approximated by the truncated Gaussian density function:

$$f(\Delta\hat{\theta}) = \begin{cases} \dfrac{1}{K_d\sqrt{2\pi\hat{\sigma}^2_{\mathrm{ML}}}} \exp\left(-\dfrac{(\Delta\hat{\theta})^2}{2\hat{\sigma}^2_{\mathrm{ML}}}\right), & \dfrac{\Delta\hat{\theta}}{\Delta\theta_{\max}} \in [-1, 1], \\ 0, & \text{others}, \end{cases} \tag{55}$$

where the truncated factor K_d is given by

$$K_d = \int_{-\Delta\theta_{\max}}^{\Delta\theta_{\max}} \frac{1}{\sqrt{2\pi\hat{\sigma}^2_{\mathrm{ML}}}} \exp\left(-\frac{(\Delta\hat{\theta})^2}{2\hat{\sigma}^2_{\mathrm{ML}}}\right) \mathrm{d}(\Delta\hat{\theta}), \tag{56}$$

and $\Delta\theta_{\max}$ may be chosen to be a value less than or equal to π but larger than a multiple of σ. For example, $\Delta\theta_{\max}$ can be taken to be half of the main-beam width.

In accordance with the above approximation and in terms of conditional expectation, three robust beamforming matrices $\boldsymbol{V}_{\mathrm{RF}}$, $\boldsymbol{v}_{\mathrm{BB}}$, and $\boldsymbol{T}_{\mathrm{BB}}$, are in order presented for HAD-based DM systems in the following.

4.1 Proposed robust analog beamforming matrix $\boldsymbol{V}_{\mathrm{RF}}$

Since we have already obtained the direction of the desired user in Section 3, a direct method to design the analog precoder is to directly implement phase alignment, which aligns the phases of phase shifters of subarray k in analog part to the direction of the desired user. The block submatrix $\boldsymbol{v}_k$ in $\boldsymbol{V}_{\mathrm{RF}}$ is given by

$$\boldsymbol{v}_{\mathrm{NRAB},k}(\hat{\theta}_{\mathrm{ML}}) = \boldsymbol{h}_k(\hat{\theta}_{\mathrm{ML}}), \tag{57}$$

where $\boldsymbol{h}_k(\cdot) = \boldsymbol{h}\left((k-1)M + 1 : kM\right)$. The phase alignment method to design the analog precoder in Eq. (57) does not take the DOA estimation error into consideration, which completely depends on the precision of DOA estimation. However, there always exists measurement error in the measured angle as

shown in Eq. (46). To combat this type of errors, we will exploit the statistical property of DOAME, i.e., its PDF to propose a robust analog beamformer (RAB). In this precoder, given the PDF of DOAME and measured DOA, using conditional expectation directly yields the following robust beamforming vector for subarray k

$$\begin{aligned}\boldsymbol{v}_{\mathrm{RAB},k} &= \mathrm{E}\{\boldsymbol{h}_k(\theta)|\hat{\theta}_{\mathrm{ML}}, f(\Delta\theta_{\mathrm{ML}})\}\\ &= \mathrm{E}_{\Delta\theta_{\mathrm{ML}}}\{\boldsymbol{h}_k(\hat{\theta}_{\mathrm{ML}} - \Delta\theta_{\mathrm{ML}})\},\end{aligned} \tag{58}$$

where the mth element of $\boldsymbol{v}_{\mathrm{RAB},k}$ is derived in Appendix A. Placing all $\boldsymbol{v}_{\mathrm{RAB},k}$ into Eq. (7), we obtain the robust analog beamforming matrix $\boldsymbol{V}_{\mathrm{RF,RAB}}$.

4.2 Proposed robust digital beamforming vector $\boldsymbol{v}_{\mathrm{BB}}$

Now, we compute the robust digital beamforming vector $\boldsymbol{v}_{\mathrm{BB}}$. Similar to [35, 38], the problem of solving $\boldsymbol{v}_{\mathrm{BB}}$ can be casted as

$$\begin{aligned}\min_{\boldsymbol{v}_{\mathrm{BB}}} \quad & \|\boldsymbol{v}_{\mathrm{FD}} - \boldsymbol{V}_{\mathrm{RF,RAB}}\boldsymbol{v}_{\mathrm{BB}}\|_2^2\\ \text{s.t.} \quad & \|\boldsymbol{V}_{\mathrm{RF,RAB}}\boldsymbol{v}_{\mathrm{BB}}\|^2 = 1,\end{aligned} \tag{59}$$

where $\boldsymbol{v}_{\mathrm{FD}}$ stands for the optimal FD beamforming vector of confidential message. Observing the above optimization problem, we find an obvious fact: if we design $\boldsymbol{v}_{\mathrm{FD}}$ well, then we easily address the problem of optimizing $\boldsymbol{v}_{\mathrm{BB}}$ with $\boldsymbol{V}_{\mathrm{RF,RAB}}$ available in the precoding subsection. Here, $\boldsymbol{v}_{\mathrm{FD}}$ is chosen to be the beamforming vector of confidential message of robust leakage method in [26].

Due to the special structure of $\boldsymbol{V}_{\mathrm{RF,RAB}}$, we have the identity $\boldsymbol{V}_{\mathrm{RF,RAB}}^{\mathrm{H}}\boldsymbol{V}_{\mathrm{RF,RAB}} = \boldsymbol{I}$, and further $\|\boldsymbol{V}_{\mathrm{RF,RAB}}\boldsymbol{v}_{\mathrm{BB}}\|^2 = \|\boldsymbol{v}_{\mathrm{BB}}\|^2 = 1$. So the optimization problem in Eq. (59) can be simplified as

$$\begin{aligned}\min_{\boldsymbol{v}_{\mathrm{BB}}} \quad & \|\boldsymbol{v}_{\mathrm{FD}} - \boldsymbol{V}_{\mathrm{RF,RAB}}\boldsymbol{v}_{\mathrm{BB}}\|_2^2\\ \text{s.t.} \quad & \|\boldsymbol{v}_{\mathrm{BB}}\|^2 = 1.\end{aligned} \tag{60}$$

According to the Lagrange multiplier method, the Lagrange function about Eq. (60) can be expressed as

$$f(\boldsymbol{v}_{\mathrm{BB}}, \lambda) = \|\boldsymbol{v}_{\mathrm{FD}} - \boldsymbol{V}_{\mathrm{RF,RAB}}\boldsymbol{v}_{\mathrm{BB}}\|_2^2 + \lambda(\boldsymbol{v}_{\mathrm{BB}}^{\mathrm{H}}\boldsymbol{v}_{\mathrm{BB}} - 1), \tag{61}$$

where λ represents the Lagrange multiplier. Taking the derivative of $f(\boldsymbol{v}_{\mathrm{BB}}, \lambda)$ with respect to $\boldsymbol{v}_{\mathrm{BB}}$ and setting it to zero, we have

$$\boldsymbol{v}_{\mathrm{BB}} = (\lambda + 1)^{-1}\boldsymbol{V}_{\mathrm{RF,RAB}}^{\mathrm{H}}\boldsymbol{v}_{\mathrm{FD}}. \tag{62}$$

Then substituting $\boldsymbol{v}_{\mathrm{BB}}$ into the constraint in Eq. (60), we have $\lambda = (\boldsymbol{v}_{\mathrm{FD}}^{\mathrm{H}}\boldsymbol{V}_{\mathrm{RF,RAB}}\boldsymbol{V}_{\mathrm{RF,RAB}}^{\mathrm{H}}\boldsymbol{v}_{\mathrm{FD}})^{-\frac{1}{2}} - 1$. Therefore, $\boldsymbol{v}_{\mathrm{BB}}$ can be expressed as

$$\boldsymbol{v}_{\mathrm{BB}} = (\boldsymbol{v}_{\mathrm{FD}}^{\mathrm{H}}\boldsymbol{V}_{\mathrm{RF,RAB}}\boldsymbol{V}_{\mathrm{RF,RAB}}^{\mathrm{H}}\boldsymbol{v}_{\mathrm{FD}})^{\frac{1}{2}}\boldsymbol{V}_{\mathrm{RF,RAB}}^{\mathrm{H}}\boldsymbol{v}_{\mathrm{FD}}. \tag{63}$$

This completes the construction of $\boldsymbol{v}_{\mathrm{BB}}$.

4.3 Proposed robust AN projection matrix $\boldsymbol{T}_{\mathrm{BB}}$

In this subsection, we will optimize the design of the digital AN projection matrix $\boldsymbol{T}_{\mathrm{BB}}$. Actually, its designing is very similar to that of $\boldsymbol{v}_{\mathrm{BB}}$ in the previous subsection. In the same fashion, after the FD AN projection matrix $\boldsymbol{T}_{\mathrm{BB}}$ is set to the robust null-space projection matrix in [26, 40], the optimization problem of finding $\boldsymbol{T}_{\mathrm{BB}}$ can be casted as

$$\begin{aligned}\min_{\boldsymbol{T}_{\mathrm{BB}}} \quad & \|\boldsymbol{T}_{\mathrm{FD}} - \boldsymbol{V}_{\mathrm{RF,RAB}}\boldsymbol{T}_{\mathrm{BB}}\|_{\mathrm{F}}^2\\ \text{s.t.} \quad & \|\boldsymbol{V}_{\mathrm{RF,RAB}}\boldsymbol{T}_{\mathrm{BB}}\|_{\mathrm{F}}^2 = 1.\end{aligned} \tag{64}$$

Because of $\|\boldsymbol{V}_{\mathrm{RF,RAB}}\boldsymbol{T}_{\mathrm{BB}}\|_{\mathrm{F}}^2 = \|\boldsymbol{T}_{\mathrm{BB}}\|_{\mathrm{F}}^2 = 1$, we can further simplify the above optimization problem as

$$\begin{aligned} \min_{\boldsymbol{T}_{\mathrm{BB}}} \quad & \|\boldsymbol{T}_{\mathrm{FD}} - \boldsymbol{V}_{\mathrm{RF,RAB}}\boldsymbol{T}_{\mathrm{BB}}\|_{\mathrm{F}}^2 \\ \text{s.t.} \quad & \|\boldsymbol{T}_{\mathrm{BB}}\|_{\mathrm{F}}^2 = 1. \end{aligned} \tag{65}$$

The objective function $\|\boldsymbol{T}_{\mathrm{opt}} - \boldsymbol{V}_{\mathrm{RF,RAB}}\boldsymbol{T}_{\mathrm{BB}}\|_{\mathrm{F}}^2$ can be represented as

$$\begin{aligned} \|\boldsymbol{T}_{\mathrm{FD}} - \boldsymbol{V}_{\mathrm{RF,RAB}}\boldsymbol{T}_{\mathrm{BB}}\|_{\mathrm{F}}^2 &= \|\mathrm{vec}(\boldsymbol{T}_{\mathrm{FD}} - \boldsymbol{V}_{\mathrm{RF,RAB}}\boldsymbol{T}_{\mathrm{BB}})\|_2^2 \\ &= \|\mathrm{vec}(\boldsymbol{T}_{\mathrm{FD}}) - \mathrm{vec}(\boldsymbol{V}_{\mathrm{RF,RAB}}\boldsymbol{T}_{\mathrm{BB}})\|_2^2 \\ &= \|\mathrm{vec}(\boldsymbol{T}_{\mathrm{FD}}) - (\boldsymbol{I}_K \otimes \boldsymbol{V}_{\mathrm{RF,RAB}})\mathrm{vec}(\boldsymbol{T}_{\mathrm{BB}})\|_2^2 \\ &= \|\boldsymbol{g} - \boldsymbol{Q}\boldsymbol{t}\|_2^2, \end{aligned} \tag{66}$$

where $\boldsymbol{g} = \mathrm{vec}(\boldsymbol{T}_{\mathrm{FD}})$, $\boldsymbol{Q} = \boldsymbol{I}_K \otimes \boldsymbol{V}_{\mathrm{RF,RAB}}$ and $\boldsymbol{t} = \mathrm{vec}(\boldsymbol{T}_{\mathrm{BB}})$. And also the constraint is reformulated as $\|\boldsymbol{t}\|_2^2 = 1$. Hence, the original optimization problem in Eq. (42) reduces to

$$\begin{aligned} \min_{\boldsymbol{T}_D} \quad & \|\boldsymbol{g} - \boldsymbol{Q}\boldsymbol{t}\|_2^2 \\ \text{s.t.} \quad & \|\boldsymbol{t}\|_2^2 = 1. \end{aligned} \tag{67}$$

It is noted that Eq. (67) has the similar form as Eq. (60). Therefore, we can similarly derived the expression of $\boldsymbol{t}$ as

$$\boldsymbol{t} = (\boldsymbol{g}^{\mathrm{H}}\boldsymbol{Q}\boldsymbol{Q}^{\mathrm{H}}\boldsymbol{g})^{\frac{1}{2}}\boldsymbol{Q}^{\mathrm{H}}\boldsymbol{g}. \tag{68}$$

Observing that $\boldsymbol{Q} = \boldsymbol{I}_K \otimes \boldsymbol{V}_{\mathrm{RF,RAB}}$, $\boldsymbol{Q}$ can be viewed as a sparse matrix due to numerous zero in it. In this case, $\boldsymbol{Q}^{\mathrm{H}}\boldsymbol{g}$ can be further written as follows:

$$\begin{aligned} \boldsymbol{Q}^{\mathrm{H}}\boldsymbol{g} &= \begin{bmatrix} \boldsymbol{V}_{\mathrm{RF,RAB}}^{\mathrm{H}} & \boldsymbol{0} & \cdots & \boldsymbol{0} \\ \boldsymbol{0} & \boldsymbol{V}_{\mathrm{RF,RAB}}^{\mathrm{H}} & \cdots & \boldsymbol{0} \\ \vdots & \vdots & & \vdots \\ \boldsymbol{0} & \boldsymbol{0} & \cdots & \boldsymbol{V}_{\mathrm{RF,RAB}}^{\mathrm{H}} \end{bmatrix} \begin{bmatrix} \boldsymbol{g}_1 \\ \boldsymbol{g}_2 \\ \vdots \\ \boldsymbol{g}_N \end{bmatrix} \\ &= \left[\boldsymbol{V}_{\mathrm{RF,RAB}}^{\mathrm{H}}\boldsymbol{g}_1, \boldsymbol{V}_{\mathrm{RF,RAB}}^{\mathrm{H}}\boldsymbol{g}_2, \ldots, \boldsymbol{V}_{\mathrm{RF,RAB}}^{\mathrm{H}}\boldsymbol{g}_N\right]^{\mathrm{T}}. \end{aligned} \tag{69}$$

Using Eq. (68) and $\boldsymbol{t} = \mathrm{vec}(\boldsymbol{T}_{\mathrm{BB}})$, the robust digital AN projection matrix $\boldsymbol{T}_{\mathrm{opt}}$ is readily gotten by just the reverse operation of matrix-to-vector operator $\mathrm{vec}(\cdot)$.

5 Simulation results and discussions

In this section, simulation results are presented to evaluate the performance of the proposed I-HAD-ESPRIT DOA estimator, its enhanced version ML-based scheme, and robust HAD-based beamforming schemes for DM. Simulation parameters are chosen as follows. The number N of antennas at Alice is 64 while Bob and Eve are single-antenna users. In sub-connected hybrid architecture, the number M of antennas in each sub-array is chosen from the set $\{4,\ 8,\ 16\}$. Besides, the number L of snapshots per DOA measurement is set to be 64 and the antenna spacing d is $\frac{\lambda}{2}$. In secure DM stage, i.e., in the second time slot, we choose the direction of desired user and eavesdropper as $\theta_d = 50^\circ$ and $\theta_e = 120^\circ$, respectively. And the PA factor β between confidential message and AN is 0.9. Besides, for the convenience of analysis, we set $\sigma_d^2 = \sigma_{\mathrm{e}}^2 = \sigma^2$.

Figure 3 demonstrates the performance of root mean squared error (RMSE) versus SNR of the proposed I-HAD-ESPRIT method with $N = 64$, $L = 64$ and $M \in \{2, 8, 16\}$. As can be seen from Figure 3, we find an interesting phenomenon that the performance gap between I-HAD-ESPRIT and hybrid CRLB becomes smaller and smaller as the value of M increases from 2 to 16. Eventually, this gap tends to zero.

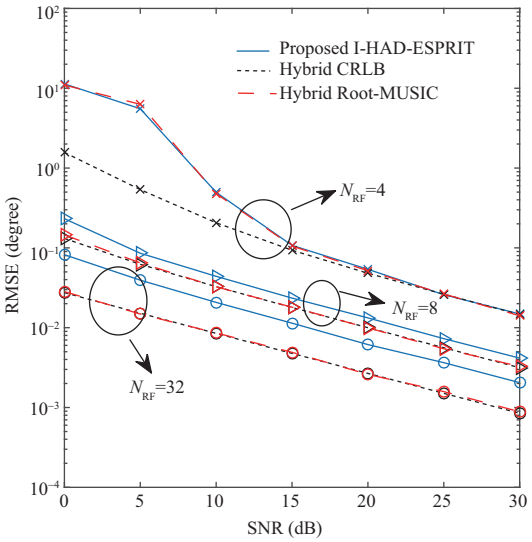

Figure 3 (Color online) RMSE versus SNR of the proposed I-HAD-ESPRIT with $N = 32$ and $M = \{4, 8, 16\}$.

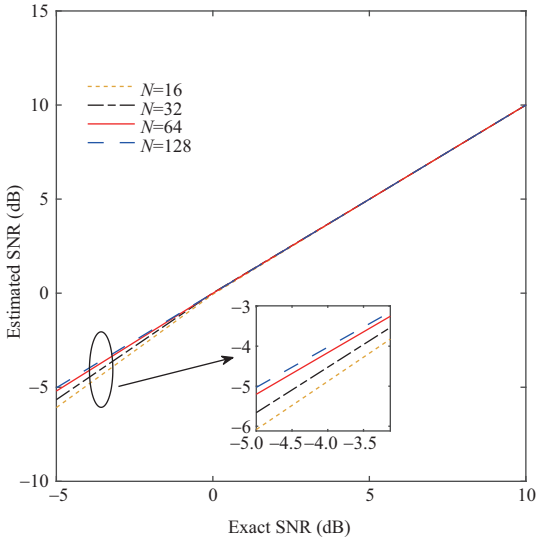

Figure 4 (Color online) Estimated SNR versus exact SNR with $M = 4$ and $N = \{16, 32, 64, 128\}$.

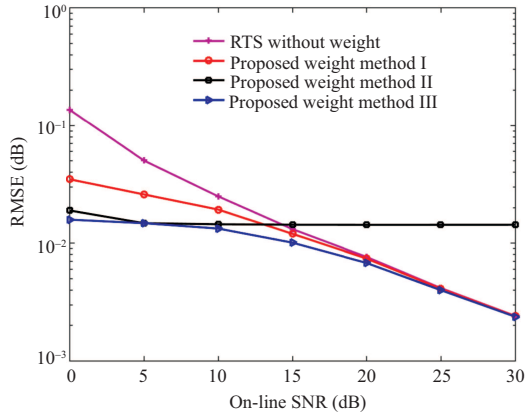

Figure 5 (Color online) RMSE versus SNR of the proposed three weight combiners of DOA ($\mathrm{SNR_{TDS}} = 10$ dB).

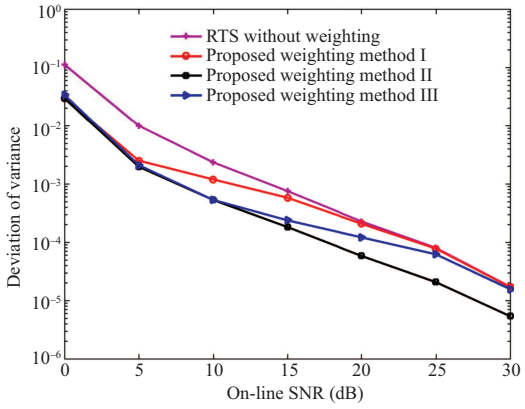

Figure 6 (Color online) RMSE versus SNR of three weight methods of estimating variance ($\mathrm{SNR_{TDS}} = 10$ dB).

And when M is up to 16 (large enough), the proposed I-HAD-ESPRIT can achieve the same performance as the hybrid root-MUSIC in [17] and achieves that of hybrid CRLB in the medium and high SNR regions. However, the proposed I-HAD-ESPRIT performs slightly worse than hybrid root-MUSIC in [17] for most cases. The main reason is as follows: when M increases, the number of RF chains will accordingly reduce such that a smaller total number of spatial-time sampling points are harvested to calculate covariance matrix of received signal.

Figure 4 plots the curves of the estimated SNR versus exact SNR with $M = 4$ and $N \in \{16, 32, 64, 128\}$. As the number of antennas increases, the estimated SNR gradually approaches the exact SNR due to the high precision of DOA estimation as the number of RF chains raises. What's more, the estimated SNR is almost coincident with the exact SNR when SNR is larger than 0 dB, in this case, the estimation error is negligible.

Figure 5 demonstrates the curves of variances of the proposed three different weight DOA combiners versus SNR for $\mathrm{SNR_{TDS}} = 5$ dB. The learning output of RTS is used as a performance upper bound. Owing to the fact that the RTS has fewer number of values of DOA measurement than TDS, it performs worst. It can be seen from Figure 5: the three proposed weight methods performs better than the

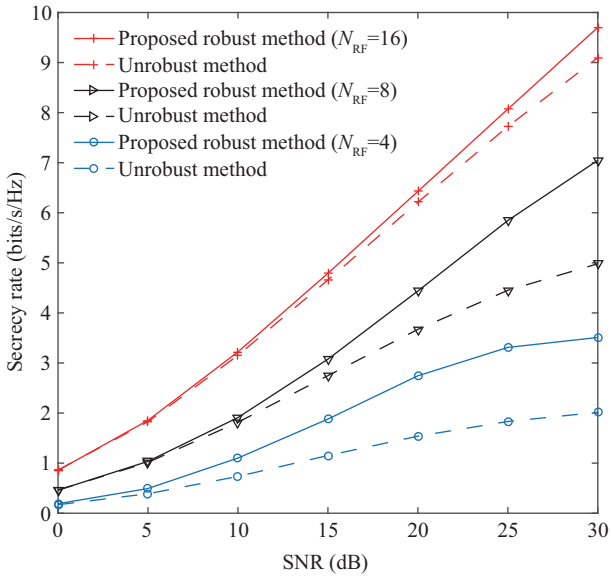

Figure 7 (Color online) Curves of SR versus SNR of the proposed robust synthesis method for HAD-based DM with $\mathrm{SNR}_{\mathrm{TDS}} = -5$ dB.

learning output of RTS without use of TDS in the low SNR region because they all fully exploit the DTS to improve the estimate precision. The proposed method III is the best one among the three proposed methods due to the fact it not only utilizes the element numbers of TDS and RTS but also exploits the SNR difference of TDS and RTS.

Figure 6 illustrates the curves of variances of the proposed three weight estimators of angle variance versus SNR with $\mathrm{SNR}_{\mathrm{TDS}} = 10$ dB. The learning output of RTS is adopted as a performance benchmark. It can be seen from Figure 6 that the proposed three weight methods exceed the learning output of RTS without using TDS in terms of variance performance. Owing to that the learning output of TDS is normalized to the same magnitude of the estimation output of RTS, the element numbers of the two sets TDS and RTS will play a dominant role in the weighting process. The result can be seen from Figure 6. That is, the proposed method II is the best one among the proposed three methods.

Figure 7 plots the curves SR versus SNR of our proposed robust synthesis method for DM using HAD structure with $\mathrm{SNR}_{\mathrm{TDS}} = -5$ dB. Here, the corresponding non-robust method is used as a performance benchmark. As can be seen from Figure 7, when DOAME exists, the proposed robust DM method always performs better than the corresponding non-robust one especially in the medium and high SNR regions. In particular, with decreasing the number of RF chains, the performance gain of the proposed robust method over nonrobust one become more obvious. In such a situation, reducing the number of RF chains, under the condition that other parameters are fixed like the receive SNR and a total number of antennas at Alice, the DOAME becomes large due to a smaller number of spatial-time sampling points available. In other words, the performance gain achieved by exploiting the density distribution of DOAME becomes more obvious in such a scenario. Otherwise, as the number of RF chains increases, a larger number of spatial-time sampling points is available to compute a high-precision variance matrix in ESPRIT. A higher-precision DOA estimation is gotten. This implies a smaller measurement error, which will accordingly decrease the performance gain achieved by the robust one proposed by us over nonrobust one.

6 Conclusion

In this paper, an I-HAD-ESPRIT DOA measurement method was proposed for HAD receiver. Here, the phase ambiguity from HAD structure has been addressed successfully. The proposed I-HAD-ESPRIT can achieve the HAD CRLB. In the mean time, we also proposed a SNR estimator. By using the proposed

I-HAD-ESPRIT method and histogram method in ML, we find an important fact that the measured DOA or DOAME follows a Gaussian distribution. Subsequently, by applying the proposed I-HAD-ESPRIT method repeatedly, we established two data sets: TDS and RTS. After the maximum likelihood learning method was optimized over TDS and RTS, we obtained the two high-precision learning outputs of DOA and variance. To combine the two learning outputs and improve performance, three weight methods were proposed to exploit the SNRs, numbers of TDS and RTS, or both. For DOA, the proposed weight method III of exploiting both is the best one among the three methods whereas the proposed weight method II is the best one among the three methods. Finally, based on the above, a robust synthesis method for HAD-based DM transmitter was proposed to exploit the density distribution of DOA measurement error, with emphasis on the design of robust analog beamforming vector. Compared to the corresponding non-robust method, the proposed robust method can achieve a substantial SR performance gain.

Acknowledgements This work was supported in part by National Natural Science Foundation of China (Nos. 61771244, 61871229).

References

1 Godara L C. Application of antenna arrays to mobile communications. II. Beam-forming and direction-of-arrival considerations. Proc IEEE, 1997, 85: 1195–1245
2 Chen J C, Yao K, Hudson R E. Source localization and beamforming. IEEE Signal Process Mag, 2002, 19: 30–39
3 Stoica P, Babu P, Li J. SPICE: a sparse covariance-based estimation method for array processing. IEEE Trans Signal Process, 2011, 59: 629–638
4 Zhang X F, Xu L Y, Xu L, et al. Direction of departure (DOD) and direction of arrival (DOA) estimation in MIMO radar with reduced-dimension MUSIC. IEEE Commun Lett, 2010, 14: 1161–1163
5 Shafin R, Liu L J, Zhang J Z, et al. DoA estimation and capacity analysis for 3-D millimeter wave massive-MIMO/FD-MIMO OFDM systems. IEEE Trans Wirel Commun, 2016, 15: 6963–6978
6 Wan L T, Han G J, Jiang J F, et al. DOA estimation for coherently distributed sources considering circular and noncircular signals in massive MIMO systems. IEEE Syst J, 2017, 11: 41–49
7 Huang H J, Yang J, Huang H, et al. Deep learning for super-resolution channel estimation and DOA estimation based massive MIMO system. IEEE Trans Veh Technol, 2018, 67: 8549–8560
8 Tuncer T E, Friedlander B. Classical and Modern Direction-of-Arrival Estimation. New York: Elsevier, 2009
9 Capon J. High-resolution frequency-wavenumber spectrum analysis. Proc IEEE, 1969, 57: 1408–1418
10 Bartlett M S. An Introduction to Stochastic Processes with Special References to Methods and Applications. New York: Cambridge University Press, 1961
11 Schmidt R. Multiple emitter location and signal parameter estimation. IEEE Trans Antenna Propag, 1986, 34: 276–280
12 Roy R, Kailath T. ESPRIT-estimation of signal parameters via rotational invariance techniques. IEEE Trans Acoust Speech Signal Process, 1989, 37: 984–995
13 Malioutov D, Cetin M, Willsky A S. A sparse signal reconstruction perspective for source localization with sensor arrays. IEEE Trans Signal Process, 2005, 53: 3010–3022
14 Hyder M M, Mahata K. Direction-of-arrival estimation using a mixed $\ell_{2,0}$ norm approximation. IEEE Trans Signal Process, 2010, 58: 4646–4655
15 Li Q L, Zhang X L, Li H. Online direction of arrival estimation based on deep learning. In: Proceedings of IEEE International Conference on Acoustics, Speech and Signal Processing (ICASSP), 2018
16 Chakrabarty S, Habets E A P. Broadband DOA estimation using convolutional neural networks trained with noise signals. In: Proceedings of IEEE Workshop on Applications of Signal Processing to Audio and Acoustics (WASPAA), 2017
17 Shu F, Qin Y L, Liu T T, et al. Low-complexity and high-resolution DOA estimation for hybrid analog and digital massive MIMO receive array. IEEE Trans Commun, 2018, 66: 2487–2501
18 Sidiropoulos N D, Bro R, Giannakis G B. Parallel factor analysis in sensor array processing. IEEE Trans Signal Process, 2000, 48: 2377–2388
19 Wang H M, Zheng T X, Yuan J, et al. Physical layer security in heterogeneous cellular networks. IEEE Trans Commun, 2016, 64: 1204–1219
20 Chen X M, Ng D W K, Gerstacker W H, et al. A survey on multiple-antenna techniques for physical layer security. IEEE Commun Surv Tut, 2017, 19: 1027–1053
21 Babakhani A, Rutledge D B, Hajimiri A. Transmitter architectures based on near-field direct antenna modulation. IEEE J Solid-State Circ, 2008, 43: 2674–2692
22 Daly M P, Bernhard J T. Directional modulation technique for phased arrays. IEEE Trans Antenna Propag, 2009, 57: 2633–2640
23 Tennant A, Shi H Z. Enhancing the security of communication via directly modulated antenna arrays. IET Microw Antenna Propag, 2013, 7: 606–611

24 Ding Y, Fusco V F. A vector approach for the analysis and synthesis of directional modulation transmitters. IEEE Trans Antenna Propag, 2014, 62: 361–370
25 Hu J S, Shu F, Li J. Robust synthesis method for secure directional modulation with imperfect direction angle. IEEE Commun Lett, 2016, 20: 1084–1087
26 Shu F, Wu X M, Li J, et al. Robust synthesis scheme for secure multi-beam directional modulation in broadcasting systems. IEEE Access, 2016, 4: 6614–6623
27 Shu F, Zhu W, Zhou X W, et al. Robust secure transmission of using main-lobe-integration-based leakage beamforming in directional modulation MU-MIMO systems. IEEE Syst J, 2018, 12: 3775–3785
28 Zhu W, Shu F, Liu T T, et al. Secure precise transmission with multi-relay-aided directional modulation. In: Proceedings of the 9th International Conference on Wireless Communications and Signal Processing (WCSP), 2017
29 Zhou X B, Li J, Shu F, et al. Secure swipt for directional modulation aided af relaying networks. 2018. ArXiv:1803.05278
30 Hu J S, Yan S H, Shu F, et al. Artificial-noise-aided secure transmission with directional modulation based on random frequency diverse arrays. IEEE Access, 2017, 5: 1658–1667
31 Shu F, Wu X M, Hu J S, et al. Secure and precise wireless transmission for random-subcarrier-selection-based directional modulation transmit antenna array. IEEE J Sel Areas Commun, 2018, 36: 890–904
32 Zhang X Y, Molisch A F, Kung S Y. Variable-phase-shift-based RF-baseband codesign for MIMO antenna selection. IEEE Trans Signal Process, 2005, 53: 4091–4103
33 Sohrabi F, Yu W. Hybrid analog and digital beamforming for mmWave OFDM large-scale antenna arrays. IEEE J Sel Areas Commun, 2017, 35: 1432–1443
34 Sohrabi F, Yu W. Hybrid digital and analog beamforming design for large-scale antenna arrays. IEEE J Sel Top Signal Process, 2016, 10: 501–513
35 Yu X H, Shen J C, Zhang J, et al. Alternating minimization algorithms for hybrid precoding in millimeter wave MIMO systems. IEEE J Sel Top Signal Process, 2016, 10: 485–500
36 Gao X Y, Dai L L, Han S F, et al. Energy-efficient hybrid analog and digital precoding for mmWave MIMO systems with large antenna arrays. IEEE J Sel Areas Commun, 2016, 34: 998–1009
37 Ramadan Y R, Minn H, Ibrahim A S. Hybrid analog-digital precoding design for secrecy mmWave MISO-OFDM systems. IEEE Trans Commun, 2017, 65: 5009–5026
38 Heath R W, Gonzalez-Prelcic N, Rangan S, et al. An overview of signal processing techniques for millimeter wave MIMO systems. IEEE J Sel Top Signal Process, 2016, 10: 436–453
39 Horn R A, Johnson C R. Pattern Recognition and Machine Learning. Berlin: Springer, 2013
40 Shu F, Wan S M, Yan S H, et al. Secure directional modulation to enhance physical layer security in IoT networks. 2018. ArXiv:1712.02104

Appendix A Derivation of RAB $\tilde{\boldsymbol{V}}_{\mathbf{RF}}$

Considering the DOA measurement error, the nonzero element of $\boldsymbol{V}_{\mathrm{RF,RAB}}$ can be represented as

$$\begin{aligned}\hat{v}_{k,m} &= \int_{-\Delta\theta_{\max}}^{\Delta\theta_{\max}} \mathrm{e}^{-\mathrm{j}\frac{2\pi d}{\lambda}[(k-1)M+m-\frac{N+1}{2}]\cos(\hat{\theta}-\Delta\theta)} \cdot p(\Delta\theta)\mathrm{d}(\Delta\theta)\\ &= \int_{-\Delta\theta_{\max}}^{\Delta\theta_{\max}} \mathrm{e}^{-\mathrm{j}\alpha_{k,m}\cos(\hat{\theta}-\Delta\theta)} \cdot p(\Delta\theta)\mathrm{d}(\Delta\theta)\\ &= \int_{-\Delta\theta_{\max}}^{\Delta\theta_{\max}} \mathrm{e}^{-\mathrm{j}\alpha_{k,m}[\cos(\hat{\theta})\cos(\Delta\theta)+\sin(\hat{\theta})\sin(\Delta\theta)]} \cdot p(\Delta\theta)\mathrm{d}(\Delta\theta),\end{aligned} \tag{A1}$$

where

$$\alpha_{k,m} = \frac{2\pi d}{\lambda}\left[(k-1)M + m - \frac{N+1}{2}\right]. \tag{A2}$$

By utilizing the second-order Taylor expansion, we can expand $\cos(\Delta\theta)$ and $\sin(\Delta\theta)$ at point $\Delta\theta = 0$ as

$$\cos(\Delta\theta) \approx 1 - \frac{1}{2}(\Delta\theta)^2, \quad \sin(\Delta\theta) \approx \Delta\theta. \tag{A3}$$

Substituting Eq. (A3) in (A1) yields

$$\begin{aligned}\hat{v}_{k,m} &= \int_{-\Delta\theta_{\max}}^{\Delta\theta_{\max}} \mathrm{e}^{-\mathrm{j}\alpha_{k,m}[\cos(\hat{\theta})\cos(\Delta\theta)+\sin(\hat{\theta})\sin(\Delta\theta)]} \cdot p(\Delta\theta)\mathrm{d}(\Delta\theta)\\ &= \int_{-\Delta\theta_{\max}}^{\Delta\theta_{\max}} \mathrm{e}^{-\mathrm{j}\alpha_{k,m}[\cos(\hat{\theta})-\cos(\hat{\theta})\cdot\frac{1}{2}(\Delta\theta)^2+\sin(\hat{\theta})(\Delta\theta)]} p(\Delta\theta)\mathrm{d}(\Delta\theta)\\ &= \xi_{k,m}\int_{-\Delta\theta_{\max}}^{\Delta\theta_{\max}} \mathrm{e}^{\mathrm{j}\alpha_{k,m}[\cos(\hat{\theta})\cdot\frac{1}{2}(\Delta\theta)^2-\sin(\hat{\theta})(\Delta\theta)]} p(\Delta\theta)\mathrm{d}(\Delta\theta)\\ &= \xi_{k,m}\int_{-\Delta\theta_{\max}}^{\Delta\theta_{\max}} \{\cos(\alpha_{k,m}\psi) + \mathrm{j}\sin(\alpha_{k,m}\psi)\} p(\Delta\theta)\mathrm{d}(\Delta\theta)\\ &= \zeta_{k,m} + \mathrm{j}\eta_{k,m},\end{aligned} \tag{A4}$$

where

$$\xi_{k,m} = \mathrm{e}^{-\mathrm{j}\alpha_{k,m}\cos(\hat{\theta})}, \tag{A5}$$

and

$$\psi = \left[\cos(\hat{\theta}) \cdot \frac{1}{2}(\Delta\theta)^2 - \sin(\hat{\theta})(\Delta\theta)\right]. \tag{A6}$$

Similarly, by utilizing the second-order Taylor expansion, $\cos(\alpha_{k,m}\psi)$ can be represented as

$$\begin{aligned}\cos(\alpha_{k,m}\psi) &= \cos\left(\alpha_{k,m}\left[\cos(\hat{\theta}) \cdot \frac{1}{2}(\Delta\theta)^2 - \sin(\hat{\theta})(\Delta\theta)\right]\right)\\ &\approx 1 - \frac{1}{2}\alpha_{k,m}^2\left[\cos(\hat{\theta}) \cdot \frac{1}{2}(\Delta\theta)^2 - \sin(\hat{\theta})(\Delta\theta)\right]^2\\ &= 1 - \frac{1}{8}\alpha_{k,m}^2\cos(\hat{\theta})^2(\Delta\theta)^4 - \frac{1}{2}\alpha_{k,m}^2\sin(\hat{\theta})^2(\Delta\theta)^2\\ &\quad + \frac{1}{2}\alpha_{k,m}^2\cos(\hat{\theta})\sin(\hat{\theta})(\Delta\theta)^3.\end{aligned} \tag{A7}$$

Since the last term of Eq. (A7) is an odd function of $\Delta\theta$, then

$$\int_{-\Delta\theta_{\max}}^{\Delta\theta_{\max}} \frac{1}{2}\alpha_{k,m}^2\cos(\hat{\theta})\sin(\hat{\theta})(\Delta\theta)^3 \cdot p(\Delta\theta)\mathrm{d}(\Delta\theta) = 0. \tag{A8}$$

Now, let us define

$$\begin{aligned}\chi_1 &= \int_{-\Delta\theta_{\max}}^{\Delta\theta_{\max}} (\Delta\theta)^4 \cdot p(\Delta\theta)\mathrm{d}(\Delta\theta)\\ &= \frac{2}{K_d\sqrt{2\pi\sigma^2}}\left\{-\sigma^2 \cdot \Delta\theta_{\max}^3\,\mathrm{e}^{-\frac{\Delta\theta_{\max}^2}{2\sigma^2}} - 3\sigma^4\Delta\theta_{\max}\mathrm{e}^{-\frac{\Delta\theta_{\max}^2}{2\sigma^2}} + \frac{3\sqrt{2\pi}}{2}\sigma^5\mathrm{erf}\left(\frac{\Delta\theta_{\max}}{\sqrt{2}\sigma}\right)\right\},\end{aligned} \tag{A9}$$

and

$$\begin{aligned}\chi_2 &= \int_{-\Delta\theta_{\max}}^{\Delta\theta_{\max}} (\Delta\theta)^2 \cdot p(\Delta\theta)\mathrm{d}(\Delta\theta)\\ &= \frac{2}{K_d\sqrt{2\pi\sigma^2}}\left\{-\sigma^2\Delta\theta_{\max} \cdot \mathrm{e}^{-\frac{\Delta\theta_{\max}^2}{2\sigma^2}} + \frac{\sqrt{2\pi}}{2}\sigma^3\mathrm{erf}\left(\frac{\Delta\theta_{\max}}{\sqrt{2}\sigma}\right)\right\}.\end{aligned} \tag{A10}$$

Then the real part $\zeta_{k,m}$ of Eq. (A4) can be expressed as

$$\zeta_{k,m} = \xi_{k,m}\left(K_d - \frac{1}{8}\alpha_{k,m}^2\cos(\hat{\theta})^2\chi_1 - \frac{1}{2}\alpha_{k,m}^2\sin(\hat{\theta})^2\chi_2\right). \tag{A11}$$

In the same manner, we can have the $\eta_{k,m}$ as follows:

$$\eta_{k,m} = \frac{1}{2}\xi_{k,m} \cdot \alpha_{k,m}\cos(\hat{\theta})\chi_2. \tag{A12}$$

Until now, we complete the derivation of $\hat{v}_{k,m}$. That is, $\hat{v}_{k,m} = \zeta_{k,m} + j\eta_{k,m}$. Owing to the special structure of analog precoder, we only need the phase of $\hat{v}_{k,m}$. Therefore we can reformulated the analog $v_{k,m}$ as

$$v_{\mathrm{RAB},k,m} = \frac{1}{\sqrt{M}}\exp(j * \angle(\hat{v}_{k,m})), \tag{A13}$$

which is what we need.